Experimental Study of Roll-formed Aluminium Lipped Channel Beams in Shear

M. Rouholamin
School of Engineering and Built Environment, Griffith University
Queensland, Australia.

S. Gunalan
School of Engineering and Built Environment, Griffith University
Queensland, Australia.

K. Poologanathan
Northumbria University, Newcastle, UK

H. Karampour
School of Engineering and Built Environment, Griffith University
Queensland, Australia.

Abstract

Use of aluminium sections as primary load bearing members has recently expanded considerably in the building industry. Aluminium as a new constructional material has several advantages in building structures including corrosion resistance, durability, high strength-to-weight ratio, reduced cost of transportation and ease of erection and fabrication. The popularity of aluminium structures has attracted attention regarding the efficiency and design of many sections, and roll-formed lipped channel beam (LCB) is one of these commonly used sections. However, aluminium LCBs are prone to shear buckling failures due to its increased web slenderness and low elastic modulus compared to steel. Hence an experimental study was conducted to investigate the shear behaviour of LCBs and to verify the current design rules to accurately predict the shear strengths. Shear tests have been conducted using ten different generally available roll-formed aluminium LCBs. The test sections were loaded at mid-span at the shear centre until failure. The results obtained from the tests were then compared with the predictions using the current shear design rules in the Australian/New Zealand standards and Eurocodes for both aluminium structures and cold-formed steel structures as their shear behaviour are quite similar. This paper presents the details and results of this experimental study and comparison with shear design rules based on current design rules.

Keywords: Roll-formed aluminium, lipped channel beams, shear behaviour, experimental study, design rules

1 Introduction

Aluminium alloy has been used in several construction applications including buildings, bridges and other special structures. The use of aluminium alloy members in the construction industry has increased during the last decade due to the improved performance of aluminium. Firstly, aluminium alloys are more durable than other building materials. They are weatherproof, corrosion-resistant, and are immune to harmful effects from UV rays; which gives a longer service life of structures compared to other materials used in the construction industry. Secondly, aluminium alloy can be extruded and rolled formed to a broad range of cross-sectional shapes, enabling aluminium alloy to be used efficiently under a wide variety of loading conditions. Thirdly, aluminium alloy has a high strength to weight ratio, which provides the strength required for the design without increasing the dead load on the structures [1]. All these features has increased the popularity of using aluminium in the construction industry.

One of the main uses of aluminium sheet is when it is forged into C-Section purlins, also known as LCBs (Figure 1). The popularity of roll-formed aluminium LCB has increased due to the efficiency and design of these sections. Hence, these sections are recently used as beams and joists in buildings. However, the vulnerability of aluminium in buckling due to low elastic modulus compared to steel and increased web slenderness of LCBs have raised the issues about the shear and web crippling failures of these sections. The web crippling behaviour and design of roll-formed aluminium LCBs were already investigated at Griffith University [3-6] and this study focus on the shear behaviour and design of these sections.

The shear behaviour of cold-formed steel sections has been extensively researched in the past. Yu and Phung [7] and LaBoube and Yu [8] studied the shear strength of cold-formed steel LCBs. They considered the web slenderness ratio, the edge support conditions and different grades of steel, in their study. Pham and Hancock [9,10] conducted a series of shear tests on cold-formed steel LCBs with various section depths and thicknesses and developed design rules as part of their study on combined bending and shear actions. Keerthan and Mahendran [11, 12] conducted a detailed experimental study to investigate the shear behaviour of hollow flange channel beams known as LiteSteel beams. They investigated the effect of different heights of the web side plates and effect of using only one web side plate, to consider practical applications. They found that reduced heights of web side plates and using one web side plate as practical support conditions were not adequate to provide the ideal simply supported

conditions and may lead to web crippling failures in the tests. A series of shear tests was further conducted by Keerthan et al. [13] to study the effect of real support conditions on the shear strength of LiteSteel beams. Keerthan and Mahendran [14] also conducted an experimental study on shear behaviour of cold-formed steel LCBs by using different web slenderness ratios and different flat width to thickness ratios.

While the shear behaviour of cold-formed steel beams has been widely researched, only limited studies have been carried out on aluminium beams. Recently an experimental study was carried out by Wang et al. [15] to investigate the shear buckling behaviour of I-shaped aluminium alloy beams under concentrated loads. Orun and Guler [16] investigated the buckling behaviour of thin-walled aluminium beams mostly used in aircraft applications under shear vertical loading. However, no research study has been conducted yet to investigate the shear behaviour of roll-formed aluminium LCBs.

Hence, an experimental study was conducted at Griffith University structural lab using ten different commonly available roll-formed aluminium LCBs to investigate the shear behaviour of these sections. The ultimate loads obtained from the experimental study were compared with the current design rules of Australian/New Zealand and European standards for both aluminium structures and cold-formed steel structures. This paper presents the details and results of this experimental study with a comparison of ultimate shear capacities obtained from tests and current design rules.

2 Experimental study

2.1 Test specimens

A total of 28 shear tests of aluminium LCBs under three-point loading was conducted to investigate the shear behaviour of these sections. An aspect ratio (shear span "a" / clear web height "d_1") of 1.0 was considered in this experimental study. Table 1 summarises the 28 tests conducted in this experimental study. Ten tests were conducted with different sections to investigate the effect of web slenderness and to cover various types of shear failure including shear yielding, inelastic shear buckling and elastic shear buckling. Three of these tests were repeated to check the reliability of the test set-up and results. Additionally, 15 tests were conducted to investigate the shear behaviour and strengths of aluminium LCBs under various test set-up and support conditions including the number of web side plates (WSP), the number

of angle straps (AS) and the number of vertical row of bolts (VRB). Further details of these specimens and test set-ups are given in Section 2.3.

The nominal web height of the ten different sections varied from 150 to 400 mm with two different nominal thicknesses (2.5 and 3.0 mm). Table 2 shows the measured dimensions of the test specimens used in this experimental study including web height (D), flange width (B), lip depth (L), web thickness (t) and internal radius of the corners (r_i). In this table D, B and L are external dimensions (Figure 1).

The specimens were labelled with specific codes, which present the conditions of the shear test assemblies based on the geometric properties and boundary conditions. For instance, "20030-2WSP-8AS-2VRB" indicates that section considered is 20030 (approximately 200 mm web height and 3.0 mm thickness). "2WSP" indicates that both sides of the section were stiffened with web side plates in the test set-up. "8AS" indicates that eight equal angle straps were used and "2VRB" shows that two vertical rows of bolts were used at the support locations to attach T-plate and web side plates.

2.2 Material properties

The test specimens were made from marine grade structural aluminium alloy 5052 H36 and their material properties were obtained by conducting tensile coupon tests of six samples of each of the ten sections based on the procedure specified in AS 1391, [17]. The coupons were taken longitudinally from the web of the specimens. A 30 kN Instron displacement-controlled testing machine was used for the coupon tests at a constant strain rate of 0.01 mm/mm/min until failure, as demonstrated in Figure 2. An extensometer was used to measure the strain during the tensile coupon test. The yield tensile strength, ultimate tensile strength and modulus of elasticity were obtained from the data recorded through tensile coupon testing. Typical stress-strain curves of the samples taken from the web element of the different sections are presented in Figure 3. Serrated yielding was observed in all the stress-strain curves as experienced in the tensile coupon tests conducted by Huynh et al. [18] on the same aluminium alloy (5052 H36).

Table 3 shows the average values of the material properties of the ten sections based on six samples per section. E, f_y and f_u are modulus of elasticity, yield (0.2% proof) and ultimate tensile stresses, respectively. Based on the table, the overall average values of E, f_y and f_u, are

68129 MPa, 225.4 MPa and 274.1 MPa, respectively. These values are used in the comparison of shear design rules with a Poisson's ratio of 0.33.

2.3 Test set-up and procedure

An experimental study was designed based on the key parameters required for shear tests in order to understand the shear behaviour of aluminium LCBs. The schematic view of the shear test set-up is shown in Figure 4. Shear test specimens were designed to fail in shear before reaching the other failure modes including torsion, web crippling and flange crushing. The test was carried out at the structural laboratory of the Griffith University using the 500 kN Material Testing System (MTS) machine.

Two aluminium LCBs were cut to the required lengths. The length of the test specimen was calculated based on the shear span 'a' (which is the distance between the centre of inner bolts on the two close web side plates as shown in Figure 4) and the width of the three web side plates (one at the middle section and at two ends of the section). The two sections were then bolted back to back via three T-shaped steel plates in the test set-up as shown in Figure 5. The gap between the back to back specimens was chosen based on the shear centre of each section. The required gap was obtained by considering the thicknesses of the T-shaped plates (40 mm) and the web side plates (10 mm or 30 mm) based on the size of the section. This consideration allows the test specimens to behave independently while loading through or near the shear centre to prevent twisting. Web side plates of 70 mm wide were used at both sides of each section at the loading point and at the two end supports to eliminate the out of plane movement of the web. Two vertical rows of M16 high tensile bolts (with hole size of 18 mm) were typically used at the loading point and two end supports. The minimum number of bolts were calculated based on the AS 4100 [19] to prevent the premature bearing failure at holes.

Since aluminium LCBs are open sections, they have an unbalanced shear flow. Hence the test specimens were restrained using angle straps to prevent any flange distortion due to the presence of the unbalanced shear flows and distortional buckling. The size of the equal angle straps was 25×25×5. The flanges of the two bolted aluminium LCBs were typically connected with eight angle straps (four at the top flanges and another four at the bottom flanges) using 32 '8G' screws as shown in Figure 5.

Five test set-up variables, which affect the shear capacity of the sections, have been investigated in this study as shown in Table 1. The schematic diagrams for these shear test set-ups are shown in Figure 6. Figure 7 shows the typical shear test set-up using web side plates on both sides and eight angle straps. Ten shear tests and three additional repeat tests were conducted using this test set-up (see Table 2). Figure 8 shows the experimental shear test set-ups using only one web side plate at the loading point and two end supports. As can be seen in the figure, the web side plate was only located behind each back to back section considering the gap related to the shear centre of the assembly. Thus, six shear tests were conducted based on this particular variable. Figure 9 shows a typical shear test assembly of aluminium LCBs without any angle straps. Angle straps are not commonly used at the loading and support points in practical applications in the building industry. Hence, six shear tests were also conducted without any angle straps. This variable was studied to investigate the effect of not having angle straps in the test set-ups on the shear behaviour and shear capacity of aluminium LCBs. Pham and Hancock [9] conducted shear tests without using angle straps at loading point. Thus, two more shear tests have been also conducted using this test set-up to investigate the shear behaviour and strengths as shown in Figure 10. Pham et al. [20] reported that using two rows of bolts at the supports as done by Keerthan and Mahendran [14] may lead to increased post buckling shear capacities of LCBs. Thus, one shear test was conducted with considering one vertical row of bolts at the two ends as shown in Figure 11 to investigate this phenomenon.

The assembled pair of aluminium LCBs was positioned accurately in the test rig with simply supported boundary conditions. The load was applied at mid-span at the shear centre by moving the cross-head of the MTS machine at a constant rate of 1 mm/minute until the test specimen failed. The MTS machine recorded the applied load and the displacement, until failure. Furthermore, four laser displacement transducers were used to record the lateral and vertical deflections of four specific points of the specimens accordingly, as shown in Figure 4. Two of the laser displacement transducers were located at the centre of the web between two web side plates (LVDT W1 and LVDT W2) to record the lateral deflection. Another two lasers were positioned under the bottom flange at the mid-span (LVDT BF) and at the top flange near the support (LVDT TF) in order to record the vertical displacement of the specimen. The shear strength (V_{ult}) of each aluminium LCB was obtained by dividing the ultimate load obtained from MTS machine by four.

2.4 Test results and discussion

The following sections present the results obtained from the experimental study including load-displacement curves, ultimate loads and failure modes.

2.4.1 Load-displacement curves

Figure 12 shows the load versus displacement curves of a typical specimen (35030-2WSP-8AS-2VRB) obtained from the four laser displacement transducers used in the shear test set-up (Figure 4). The bottom flange laser (LVDT BF) presents the vertical displacement of the specimen at the mid-span. The vertical displacement from top flange laser (LVDT TF) measured at the top flange shows that the test assembly did not slip at the end supports through the bolt holes. The behaviour of the load versus lateral displacements of the webs measured by lasers (LVDT W1 and LVDT W2) are quite similar. Figure 13 further analyses the load versus lateral deflection of LVDT W2. The web began to deflect out of plane at 47.6 kN at Point 1 and this load value was considered as the elastic buckling load from the test. Then the beam reached the ultimate shear capacity of 85.01 kN at Point 2 indicating a very high post buckling strength for aluminium LCBs due to tension field action. Currently there is no literature or standard available on this phenomenon for Aluminium LCBs. However, Keerthan and Mahendran [14] also observed a very similar behaviour for cold-formed steel LCBs. Figure 13 shows the elastic buckling loads obtained from AS/NZS 4600 [21] (42.2 kN) and Keerthan and Mahendran [14] (45.6 kN) using the aluminium properties. It was found that the elastic buckling load predicted by Keerthan and Mahendran [14] was close to the buckling load obtained from the test as shown in Figure 13. This is due to the fact that Keerthan and Mahendran [14] considered the fixity provided by the flanges to the webs of LCBs in calculating the shear buckling coefficients (discussed further in Section 3.2.1).

Figure 14 presents the load versus lateral deflection curves for a typical section (25025) with different shear test set-ups. The assembly with two web side plates (2WSP) and eight angle straps (8AS) were comparatively rigid than other assemblies with one web side plate (1WSP) or reduced angle straps (6AS or 0AS). There was not any behavioural difference between the assemblies with one and two vertical rows of bolts. Figure 14 also shows that the lateral deflection was the highest when one web side plate was used. Figure 15 presents the load versus vertical displacement graphs obtained from five different shear test set-ups for Section 25025. The test set-up of 2WSP-8AS-2VRB was the stiffest compared to other test assemblies. Even though the test assembly with one and two vertical rows of bolts (1VRB and 2VRB) behaved

similarly in Figure 14, they were different in Figure 15. This is due to the difference in the fixity provided at the end supports by these two different boundary conditions.

2.4.2 Ultimate loads

Table 4 presents the ultimate shear loads for ten different sections obtained from the shear tests using web side plates on both sides, eight angle straps at the top and bottom flanges and two vertical rows of bolts at support locations (2WSP-8AS-2VRB). The percentage difference between the repeated tests of 15025, 15030 and 35030 were 4%, 1% and 1%, respectively indicating the reliability of the experimental study.

Table 5 presents the ultimate loads of aluminium LCBs for other boundary conditions (1WSP-8AS-2VRB, 2WSP-0AS-2VRB, 2WSP-6AS-2VRB, 2WSP-8AS-1VRB). As expected, these ultimate loads are comparatively lower than the values obtained for the boundary condition 2WSP-8AS-2VRB. Hence the ratios of ultimate loads compared to (2WSP-8AS-2VRB) are also presented in this table to predict the reduction in shear strengths due to various boundary conditions. The ultimate loads reduced by 4% to 9% (average = 5%) when one web side plate was used (1WSP-8AS-2VRB) compared to the shear tests where web side plates were used on both sides (2WSP-8AS-2VRB). Further, the ultimate loads reduced by 7% to 16% (average = 10%) when angle straps were not used (2WSP-0AS-2VRB) compared to the shear tests where eight angle straps were used (2WSP-8AS-2VRB). This observation is similar to the shear test results obtained by Keerthan and Mahendran [14] where 9 to 20% reduction in shear capacity was observed in cold-formed steel LCBs without any angle straps compared with specimens having eight angle straps. The shear capacities of those sections using six angle straps (2WSP-6AS-2VRB) are not very different compared with the results of those using eight angle straps (2WSP-8AS-2VRB). In addition, the shear capacities of those sections using only one vertical rows (2WSP-8AS-1VRB) are not very different compared with results of those using two vertical rows of bolts (2WSP-8AS-2VRB). It should be noted that Pham and Hancock [22] evaluated the effect of varying the number of horizontal bolt lines on the tension field, whereas in the present work a variation on the number of vertical bolt lines was made at the supports. The significant effect on the development of the tension field is the removal of horizontal bolt lines in the diagonally tensioned regions in which the tension field is anchored. Hence the influence of the number of vertical rows of bolts on the shear strengths of aluminium LCBs is insignificant.

2.4.3 Failure modes

Figure 16 shows the shear failure modes of section 25025 using five different shear test set-ups. Figure 16(a) presents the shear failure mode of specimens using web side plates on both sides and eight angle straps. Figure 16(b) also shows a similar failure mode with one vertical row of bolts at the two ends. Figure 16(c) shows the shear failure mode of test set-up using only one web side plate. It was found that the cross-section of the specimen moved at the top and bottom flanges. The top side moved towards the shear centre and the bottom side moved away from the shear centre, in both back to back sections of the assembly, which resulted in shear capacity reduction. Figures 16(d) and (e) present the failure modes for the shear test set-up without any angle straps and six angle straps, respectively. Flange distortion is observed relatively more in 2WSP-0AS-2VRB compared to 2WSP-6AS-2VRB.

3 Current shear design rules

The nominal shear capacities of LCBs can be obtained using AS/NZS 1664.1 [23] and Eurocode 9 Part 1-4 [24] for aluminium structural members or AS/NZS 4600 [21] and Eurocode 3 Part 1-3 [25] for cold-formed steel structural members.

3.1 Aluminium structures

3.1.1 AS/NZS 1664.1 [23]

The nominal shear strength V_v in aluminium structures can be determined using Equations (1), (2) and (3) based on the Australian/New Zealand standard (AS/NZS 1664.1).

$$V_v = V_y = F_{sy} d_1 t \quad ; \text{ for } \frac{a_e}{t} < S_1 \tag{1}$$

$$V_v = 1.375[B_s - 1.25 D_s(\frac{a_e}{t})] d_1 t \quad ; \text{ for } S_1 < \frac{a_e}{t} < S_2 \tag{2}$$

$$V_v = \frac{1.375\pi^2 E}{(1.25\frac{a_e}{t})^2} d_1 t \quad ; \text{ for } S_2 < \frac{a_e}{t} \tag{3}$$

in which

$$B_s = F_{sy}[1 + \frac{(F_{sy})^{\frac{1}{3}}}{11.8}] \quad ; \text{ intercept, MPa} \tag{4}$$

$$D_s = \frac{B_s}{20}(\frac{6B_s}{E})^{\frac{1}{2}} \quad ; \text{ slope, MPa} \tag{5}$$

$$C_s = \frac{2B_s}{3D_s} \quad ; \text{ intersection} \tag{6}$$

$$S_1 = \frac{B_s - \frac{F_{sy}}{1.375}}{1.25 D_s} \quad ; \text{ first slenderness limit} \tag{7}$$

$$a_e = \frac{a_1}{\sqrt{1+0.7(\frac{a_1}{a_2})^2}} \tag{8}$$

where a_1 is the shorter dimension of rectangular panel and a_2 is the longer dimension of rectangular panel. F_{sy} is the shear yield strength, d_1 is the clear web depth ($d_1 = D - 2t - 2r_i$), t is the web thickness, r_i is the internal radius, E is modulus of elasticity and S_2 is the second slenderness limit ($S_2 = \frac{a_e}{t}$) at the intersection of Equations (2) and (3).

3.1.2 Eurocode 9 [24]

The nominal shear capacities of aluminium LCBs can be obtained using Eurocode 9 Part 1-4 for aluminium structural members. The shear design resistance of webs where the transverse stiffeners are used at the supports are obtained as follows using Equations (9), (10) and (11).

$$V_v = V_y = \frac{0.58 f_y h_w t}{sin\phi} \quad ; \text{ for } \lambda_w \leq 0.83 \tag{9}$$

$$V_v = \frac{0.48 f_y h_w t}{\lambda_w sin\phi} \quad ; \text{ for } 0.83 < \lambda_w < 1.4 \tag{10}$$

$$V_v = \frac{0.48 f_y h_w t}{\lambda_w sin\phi} \quad ; \text{ for } \lambda_w \geq 1.4 \tag{11}$$

$$\text{in which} \quad \lambda_w = 0.346 \frac{S_w}{t} \sqrt{\frac{f_y}{E}} \tag{12}$$

where f_y is the yield strength, h_w is web height between the midlines of the flanges ($h_w = D - t$), λ_w is slenderness ratio, ϕ is the slope of the web relative to the flanges ($\phi = 90°$ for LCBs) and S_w is the distance between the midpoints of the corners ($S_w = D - t - 2r_m (1 - \text{Sin } 45°)$) where $r_m = r_i + t/2$ (see Figure 17).

3.2 Cold-formed steel structures

3.2.1 Current AS/NZS 4600 [21]

The nominal shear capacity V_v of cold-formed steel channel sections can be determined using Equations (13), (14) and (15).

$$V_v = V_y = 0.64 f_y d_1 t \quad ; \text{ for } \frac{d_1}{t} \leq \sqrt{\frac{E k_v}{f_y}} \tag{13}$$

$$V_v = 0.64 t^2 \sqrt{E k_v f_y} \quad ; \text{ for } \sqrt{\frac{E k_v}{f_y}} < \frac{d_1}{t} \leq 1.415 \sqrt{\frac{E k_v}{f_y}} \tag{14}$$

$$V_v = \frac{k_v \pi^2 E t^3}{12(1-v^2)d_1} \quad ; \text{ for } \frac{d_1}{t} > 1.415\sqrt{\frac{Ek_v}{f_y}} \tag{15}$$

where v is the Poisson's ratio and k_v is the shear buckling coefficient for stiffened webs calculated as follows:

$$k_v = 4.00 + \left[\frac{5.34}{(\frac{a}{d_1})^2}\right] \quad ; \text{ for } \frac{a}{d_1} \leq 1.0 \tag{16}$$

$$k_v = 5.34 + \left[\frac{4}{(\frac{a}{d_1})^2}\right] \quad ; \text{ for } \frac{a}{d_1} > 1.0 \tag{17}$$

in which a is the distance between transverse stiffeners on the web of the channel section.

In the traditional method of shear design of cold-formed steel LCBs, the shear buckling behaviour of web is investigated in isolation without the effect of flange rigidity. Hence Keerthan and Mahendran [14] modified the current shear design rules of AS/NZS 4600 for cold-formed steel channel sections using Equations (18), (19) and (20) where k_{LCB} is the shear buckling coefficient for LCBs with stiffened webs.

$$V_v = V_y \quad ; \text{ for } \frac{d_1}{t} \leq \sqrt{\frac{Ek_{LCB}}{f_y}} \tag{18}$$

$$V_v = V_i + 0.2(V_y - V_i) \quad ; \text{ for } \sqrt{\frac{Ek_{LCB}}{f_y}} < \frac{d_1}{t} \leq 1.508\sqrt{\frac{Ek_{LCB}}{f_y}} \tag{19}$$

$$V_v = V_{cr} + 0.2(V_y - V_{cr}) \quad ; \text{ for } \frac{d_1}{t} > 1.508\sqrt{\frac{Ek_{LCB}}{f_y}} \tag{20}$$

in which $V_y = 0.6 f_y d_1 t$ (21)

$$V_i = 0.6t^2\sqrt{Ek_v f_y} \tag{22}$$

$$V_{cr} = \frac{k_v \pi^2 E t^3}{12(1-v^2)d_1} \tag{23}$$

$$k_{LCB} = k_{ss} + 0.23(k_{sf} - k_{ss}) \tag{24}$$

where k_{sf} and k_{ss} are the coefficient of shear buckling of web of the channel sections with simple-fixed and simple-simple boundary conditions. k_{ss} is equal to k_v (Equations (16) and (17)) and k_{sf} can be calculated using Equations (25) and (26).

$$\text{where } k_{sf} = \frac{5.34}{(\frac{a}{d_1})^2} + \frac{2.31}{(\frac{a}{d_1})} - 3.44 + 8.39\,(\frac{a}{d_1}) \quad ; \text{ for } \frac{a}{d_1} < 1 \tag{25}$$

$$k_{sf} = 8.98 + \frac{5.61}{(\frac{a}{d_1})^2} - \frac{1.99}{(\frac{a}{d_1})^3} \quad ; \text{ for } \frac{a}{d_1} \geq 1 \tag{26}$$

3.2.2 Direct Strength Method [21, 26]

The Direct Strength Method (DSM) provides a simple design form to determine the shear capacity of structural sections. The DSM was formally adopted in AS/NZS 4600, and it simplifies the design stress calculation of a given section using the elastic buckling stress of the entire section. Pham and Hancock [22] showed that considerable tension field action is available for local buckling if the web is fully restrained at the loading and support points over its full depth by bolted connections. This post-local buckling has been included in the recent DSM equations in AS/NZS 4600 [21] and AISI [26]. The current DSM equations to predict the shear capacities of cold-formed steel sections which include the tension field action are as follows [21, 26]:

$$\frac{V_v}{V_y} = 1 \quad ; \text{ for } \lambda_v \leq 0.776 \tag{27}$$

$$\frac{V_v}{V_y} = [1 - 0.15\left(\frac{V_{cr}}{V_y}\right)^{0.4}](\frac{V_{cr}}{V_y})^{0.4} \quad ; \text{ for } \lambda_v > 0.776 \tag{28}$$

where

$$\lambda_v = \sqrt{\frac{V_y}{V_{cr}}} \tag{29}$$

$$V_y = 0.6 f_y d_1 t \tag{30}$$

$$V_{cr} = \frac{k_{LCB}\pi^2 E t^3}{12(1-v^2)d_1} \tag{31}$$

Keerthan and Mahendran [27] claimed that in these equations, a power coefficient of ‘‘*n*’’, which is used as 0.4 in current design rules, should be different. It was proposed that it can be taken conservatively as 0.55 for cold-formed steel LCBs based on their test and FEA results reported in Keerthan and Mahendran [14, 28]. Their modified DSM design rules are as follows:

$$\frac{V_v}{V_y} = 1 \quad ; \text{ for } \lambda_v \leq 0.815 \tag{32}$$

$$\frac{V_v}{V_y} = [1 - 0.15\left(\frac{V_{cr}}{V_y}\right)^{0.55}](\frac{V_{cr}}{V_y})^{0.55} \quad ; \text{ for } \lambda_v > 0.815 \tag{33}$$

where λ_v is non-dimensional slenderness using Equation (29), V_y is yield shear force using Equation (30) and V_{cr} is elastic shear buckling force determined using Equation (31).

3.2.2 Eurocodes 3 [25]

The shear design rules for cold-formed steel structures in Eurocode 3 Part 1-3 are similar to aluminium structures in Eurocode 9 Part 1-4 which is discussed in Section 3.1.2.

3.3 Comparison of test results with current design rules

The ultimate loads obtained from the experimental study were compared with the current design rules. Figures 18 to 22 show the non-dimensional shear capacity curves for aluminium LCBs based on AS/NZS 1664.1 [23], Eurocode 9 [24], AS/NZS 4600 [21], Keerthan and Mahendran [14] and DSM [21,14], respectively.

Figure 18 demonstrates that the current design rules of AS/NZS 1664.1 [23] over predicts the shear capacities of some sections (for a_e/t ratio between 45 to 80), but conservative otherwise. Figure 19 shows that current shear design rules of Eurocode 9 are too conservative for all the aluminium LCBs considered in the study. The current design rules of AS/NZS 4600 [21] and the modified design rules by Keerthan and Mahendran [14] are reliable for compact sections but too conservative for slender sections (for d_1/t ratio greater than 80) as shown in Figures 20 and 21. Figure 22 presents the recent DSM design rules given in AS/NZS 4600 [21] and the modified ones by Keerthan and Mahendran [14]. It should be noted that the recent DSM design rules in AS/NZS 4600 [21] includes the tension field effect for beams with slender webs. Hence it was found that these design rules agree well with the experimental results as shown in Figure 22. Similar findings were observed in the shear tests conducted by Silva and Malite [29] on plain web Z-sections.

Table 6 presents the results of the first ten shear tests (2WSP-8AS-2VRB) with predicted shear capacities obtained from current shear design rules of AS/NZS 1664.1 [23], Eurocode 9 [24], AS/NZS 4600 [21] and modified design rules of AS/NZS 4600 (Keerthan and Mahendran [14]). Although AS/NZS 1664.1 has an appropriate mean value of 0.99, it is unreliable due to the high coefficient of variation (COV) of 0.142. It was found that the current shear design rules of AS/NZS 4600 and Eurocode 9 are not in good agreement with the tests results with mean values of 1.55 and 1.42 and COVs of 0.128 and 0.307, respectively. However, the recent DSM design rules in AS/NZS 4600 [21] with tension field effect were found to be reliable based on the mean value and COV, 1.05 and 0.035, respectively.

Based on the results obtained from this experimental study (Section 2.4.2), the reduction factors of 0.95 or 0.90 could be used with Equations (18) – (20) to estimate the ultimate shear strengths of aluminium LCBs (without ideal boundary conditions but) with one web side plate (1WSP-8AS-2VRB) or without any angle straps (2WSP-0AS-2VRB), respectively. Table 7 presents the comparison of test results with reduction factors and DSM [21, 26] for these boundary conditions. It was found that the proposed reduction factors and the DSM [21, 26] reasonably predict the shear strengths of aluminium LCBs with respective boundary conditions.

4 Conclusion

This paper presented an experimental study of roll-formed aluminium LCBs to investigate the shear behaviour and strengths of these sections. Ten different sections were considered with five different boundary conditions to understand the influence of shear test set-ups on the behaviour and strengths of aluminium LCBs. On average, it was found that the shear strengths reduced by 10% for the tests with one web side plate compared to the ones with web side plates on both sides. Similarly, the shear strengths reduced marginally by 5% when angle straps were not used in the test assembly compared to ones with eight angle straps. The ultimate loads obtained from the tests were compared with the current shear design rules of Australian/New Zealand standard and Eurocode for both aluminium structure and cold-formed steel structure, as their shear behaviour are quite similar. The comparison showed that the current shear design rules are not reliable to predict the shear capacity of aluminium LCBs. AS/NZS 1664.1 was found to be over predicting the capacities for some sections and Eurocode 9 was too conservative for both compact and slender sections. The current shear design rules of AS/NZS 4600 were also too conservative in predicting the shear capacity of aluminium LCBs for slender sections. However, the recent DSM design rules in AS/NZS 4600 which considers the tension field effect were able to accurately predict the shear capacities of aluminium LCBs.

Acknowledgments

The authors wish to thank Griffith University for providing the necessary facilities and support, and Mr Robert Price from BlueScope Building Components Pty Ltd for supplying the test specimens.

References

[1] Su M.N., Young B., Gardner L. (2014), Deformation-based design of aluminium alloy beams, Engineering structures, 80 (1), 339 – 349.

[2] DIY Trade (2013), Global B2B Trading Platform, retrieved 22 August 2013, <https://img.diytrade.com/cdimg/2107209/33285228/0/1376876432/Ground_mounting_aluminum_roof_solar_mounting_bracket.jpg >.

[3] Alsanat, H. Gunalan, S. Guan, H. Keerthan, P. and Bull J. (2019), Experimental study of aluminium lipped channel sections subjected to web crippling under two flange load cases, Thin-walled structures, 141, 460-476.

[4] Alsanat, H. Gunalan, S. Keerthan, P. Guan, H. and Tsavdaridis, KD. (2019), Web crippling behaviour and design of aluminium lipped channel sections under two flange loading conditions, Thin-walled structures, 144, 106265.

[5] Alsanat, H. Gunalan, S. Keerthan, P. Guan, H. and Baniotopoulos, C. (2019), Web crippling for fastened aluminium lipped channel sections under two flange loading conditions, Journal of structural engineering, 146 (4), 04020023.

[6] Alsanat, H. Gunalan, S. Keerthan, P. Guan, H., Tsavdaridis KD. (2019), Numerical investigation of web crippling in fastened aluminium lipped channel sections under two-flange loading conditions, Structures, 23, 351-365.

[7] Yu W., Phung N. (1978), Webs for cold formed steel flexural members structural behavior of transversely reinforced beam webs. Research report. American iron and steel institute, University of missouri-rolla, Rolla, USA.

[8] LaBoube R.A., Yu W.W. (1978), Cold-formed steel beam webs subjected primarily to shear. Research report. American iron and steel institute, University of missouri-rolla, Rolla, USA.

[9] Pham C.H., Hancock G.J. (2010), Experimental investigation of high strength cold-formed c-sections in combined bending and shear, Journal of structural engineering, 136 (7), 866 – 878.

[10] Pham C.H., Hancock G.J. (2012), Direct strength design of cold-formed c-sections for shear and combined actions, Journal of structural engineering, 138 (6), 759 – 768.

[11] Keerthan P., Mahendran M. (2010), Experimental studies on the shear behaviour and strength of LiteSteel beams, Engineering structures, 32 (10), 3235 – 3247.

[12] Keerthan P., Mahendran M. (2011), New design rules for the shear strength of LiteSteel beams, Journal of constructional steel research, 67 (6), 1050 – 1063.

[13] Keerthan P., Mahendran M., Narsey A. (2015), Shear tests of hollow flange channel beams with real support conditions, Structures, 3 (1), 109 – 119.

[14] Keerthan P., Mahendran M. (2015), Experimental investigation and design of lipped channel beams in shear, Thin-walled structures, 86 (1), 174 – 184.

[15] Wang Y.Q., Wang Z.X., Yin F.X., Shi Y.J., Yin J. (2016), Experimental study and finite element analysis on the local buckling behaviour of aluminium alloy beams under concentrated loads, Thin-walled structures, 105 (1), 44 – 56.

[16] Orun A.E., Guler M.A. (2017), Effect of hole reinforcement on the buckling behaviour of thin-walled beams subjected to combined loading, Thin-walled structures, 118 (1), 12 – 22.

[17] Standards Australia (2007), Metallic materials - Tensile testing at ambient temperature, AS1391, Sydney, Australia.

[18] Huynh L.A.T., Pham C.H., Rasmussen K.J.R. (2019), Mechanical properties and residual stresses in cold-rolled aluminium channel sections, Engineering structures, 199 (1).

[19] Standards Australia (SA) (1998), Steel structures, AS 4100, Sydney, Australia.

[20] Pham S.H., Pham C.H., Rogers C.A., Hancock G.J. (2019), Experimental validation of the Direct Strength Method for shear spans with high aspect ratios, Journal of constructional steel research, 157 (1), 143 – 150.

[21] Standards Australia (SA) (2018), Cold-formed steel structures, AS/NZS 4600, Sydney, Australia.

[22] Pham C.H., Hancock G.J. (2012), Tension field action for cold-formed sections in shear, Journal of constructional steel research, 72 (1), 168 – 178.

[23] Standards Australia (SA) (1997), Aluminium structures - Part 1: Limit state design, AS/NZS 1664.1, Sydney, Australia.

[24] European Committee for Standardization (CEN) (2007), Design of aluminium structures - Part 1.4: Cold-formed structural sheeting, Eurocode 9, Brussels, Belgium.

[25] European Committee for Standardization (CEN) (2006), Design of steel structures - Part 1.3: General rules-Supplementary rules for cold-formed members and sheeting, Eurocode 3, Brussels, Belgium.

[26] AISI (2016), North American specification for the design of cold-formed steel structural members, American iron and steel institute, 2016 Edition, Washington DC.

[27] Keerthan P., Mahendran M. (2015), Improved shear design rules of cold-formed steel beams, Engineering structures, 99 (1), 603 – 615.

[28] Keerthan P., Mahendran M. (2014), Numerical modelling and design of lipped channel beams subject to shear, In: Proceedings of the 7th European conference on steel and composite structures, Napoli, Italy, 445 – 446.

[29] Silva, J.M.M., Malite, M. (2020), Longitudinally stiffened web purlins under shear and bending moment, Thin-walled structures, 148 (1), 106616.

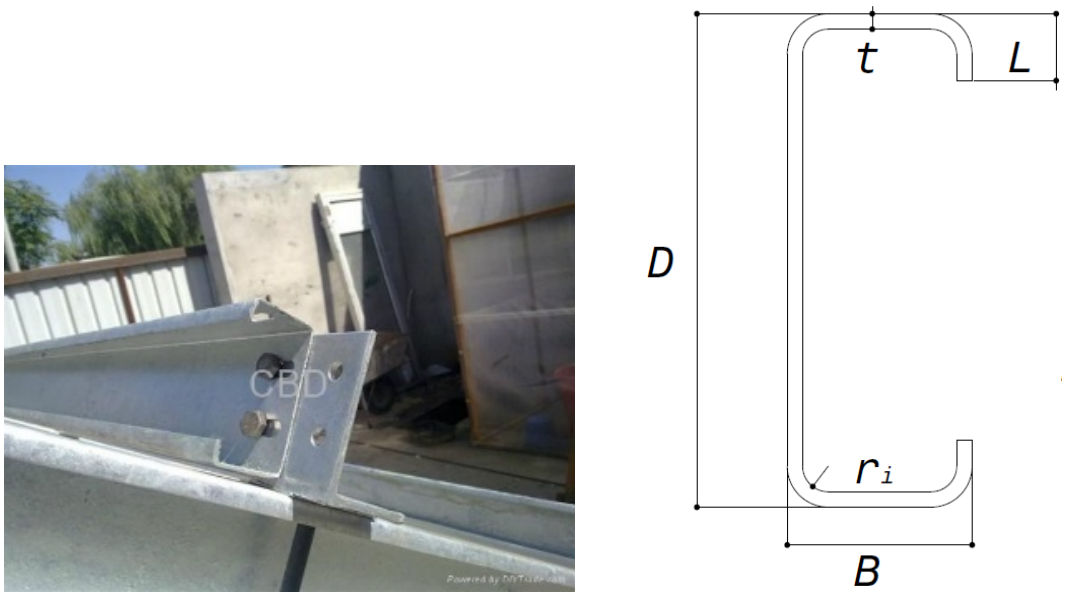

Figure 1: Application of roll-formed aluminium sections as flexural member, DIY Trade [2].

Figure 2: Tensile coupon test set-up.

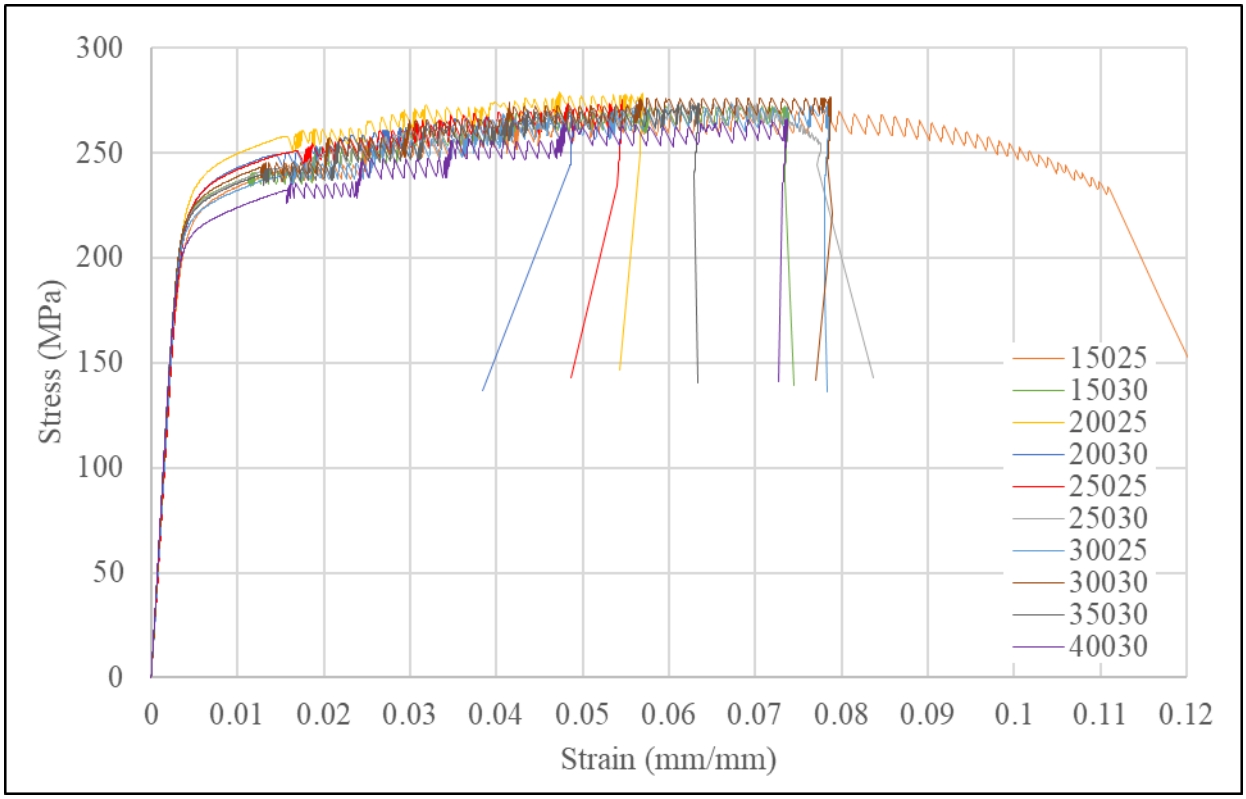

Figure 3: A stress-strain response of aluminium LCBs obtained from tensile coupon test.

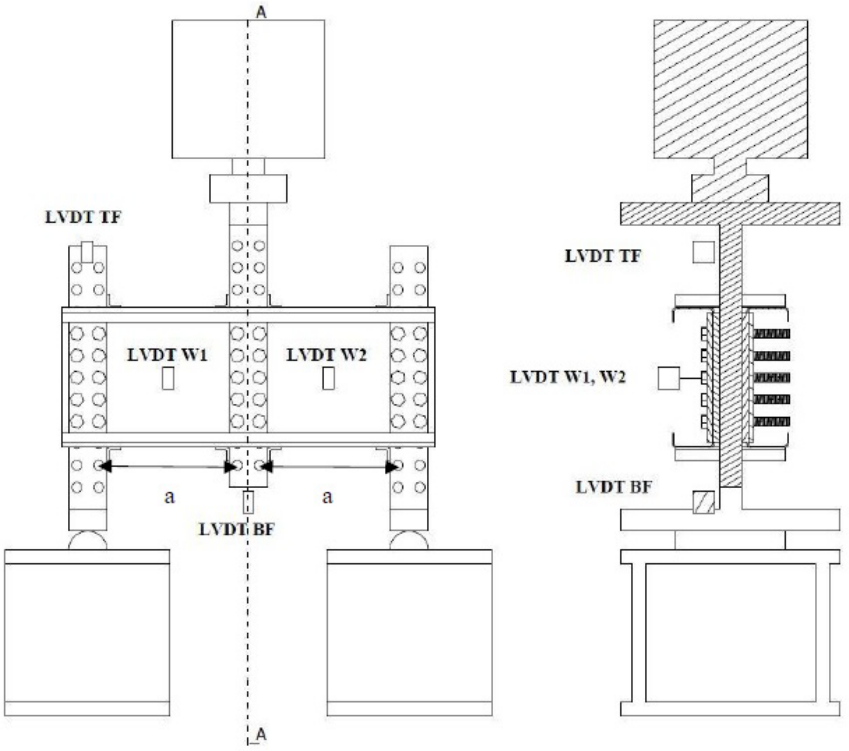

(a) Front view (b) Section A-A

Figure 4: Schematic view of the test set-up.

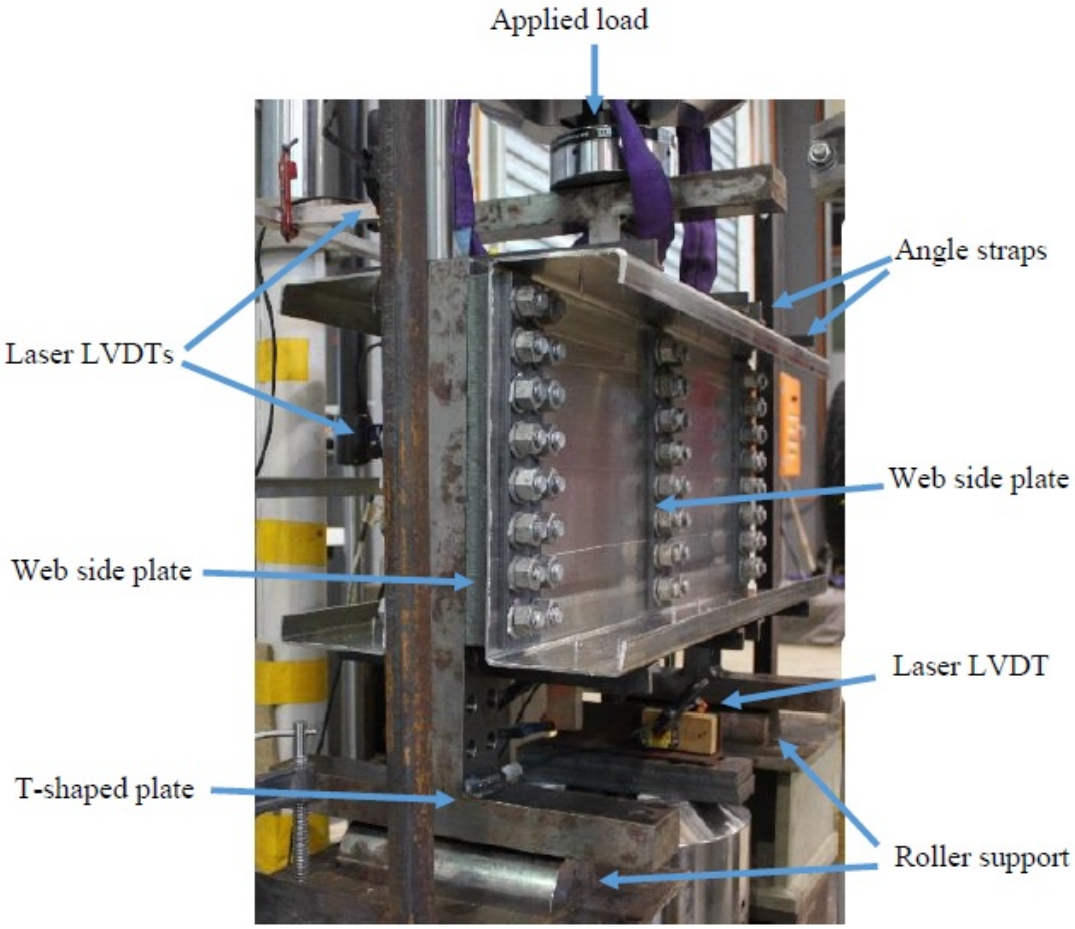

Figure 5: Experimental test set-up.

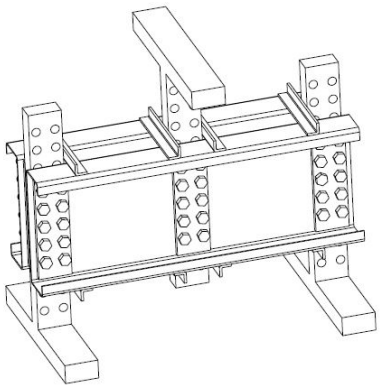

(a) 2WSP-8AS-2VRB

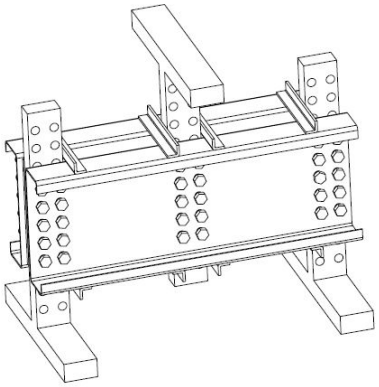

(b) **1WSP**-8AS-2VRB

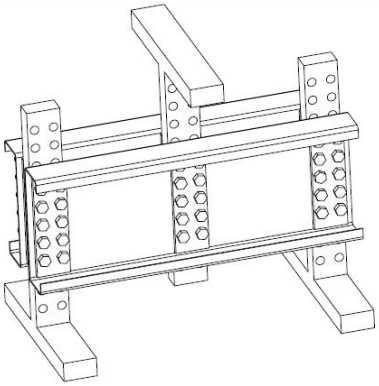

(c) 2WSP-**0AS**-2VRB

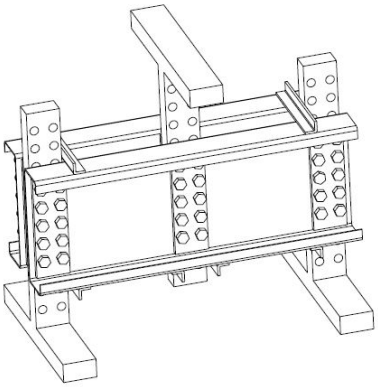

(d) 2WSP-**6AS**-2VRB

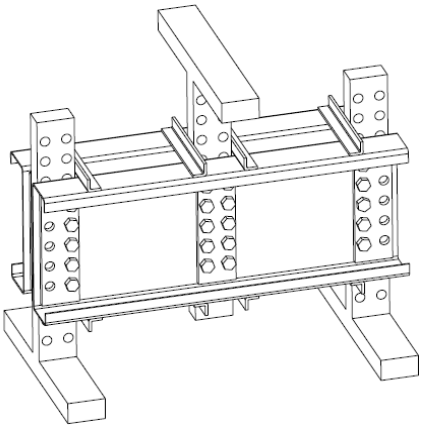

(e) 2WSP-8AS-**1VRB**

Figure 6: Schematic views of five shear test set-ups for section 25025.

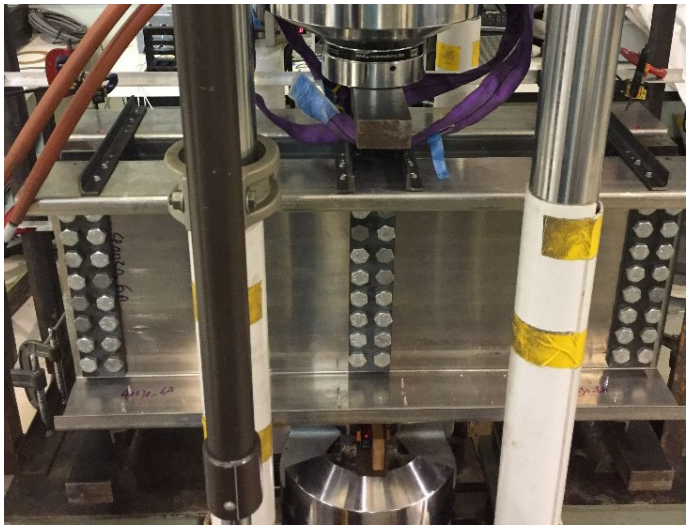

Figure 7: Shear test assembly of 40030-2WSP-8AS-2VRB.

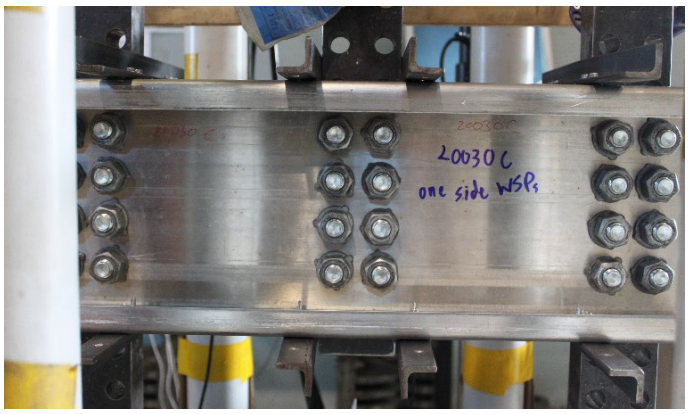

Figure 8: Shear test assembly of 20030-1WSP-8AS-2VRB.

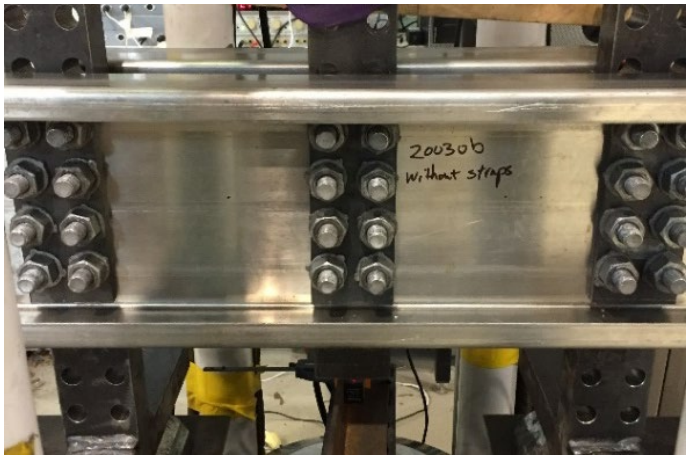

Figure 9: Shear tests assembly of 20030-2WSP-0AS-2VRB.

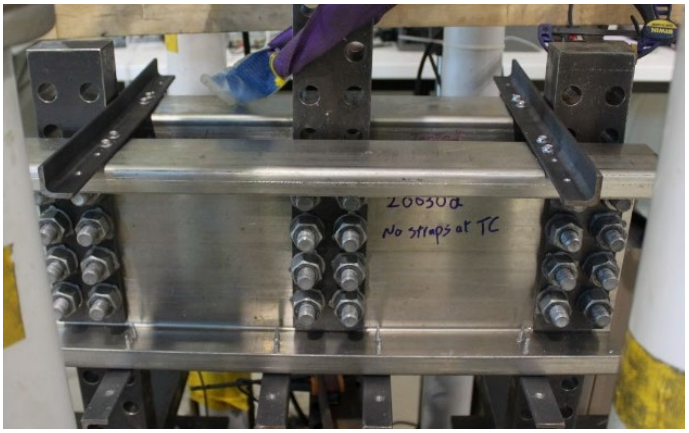

Figure 10: Shear tests assembly of 20030-2WSP-6AS-2VRB.

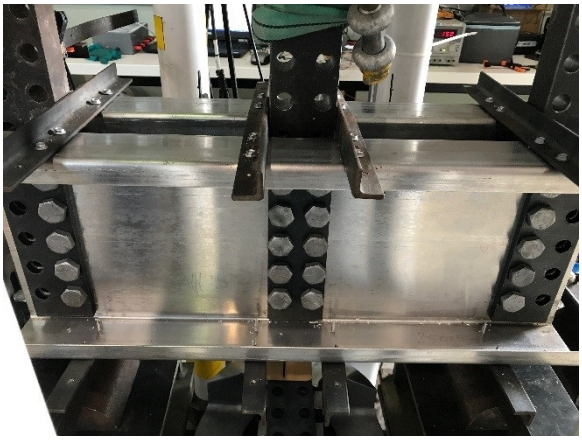

(a) Test set-up

(b) Support condition

Figure 11: Shear tests assembly of 25025-2WSP-8AS-1VRB.

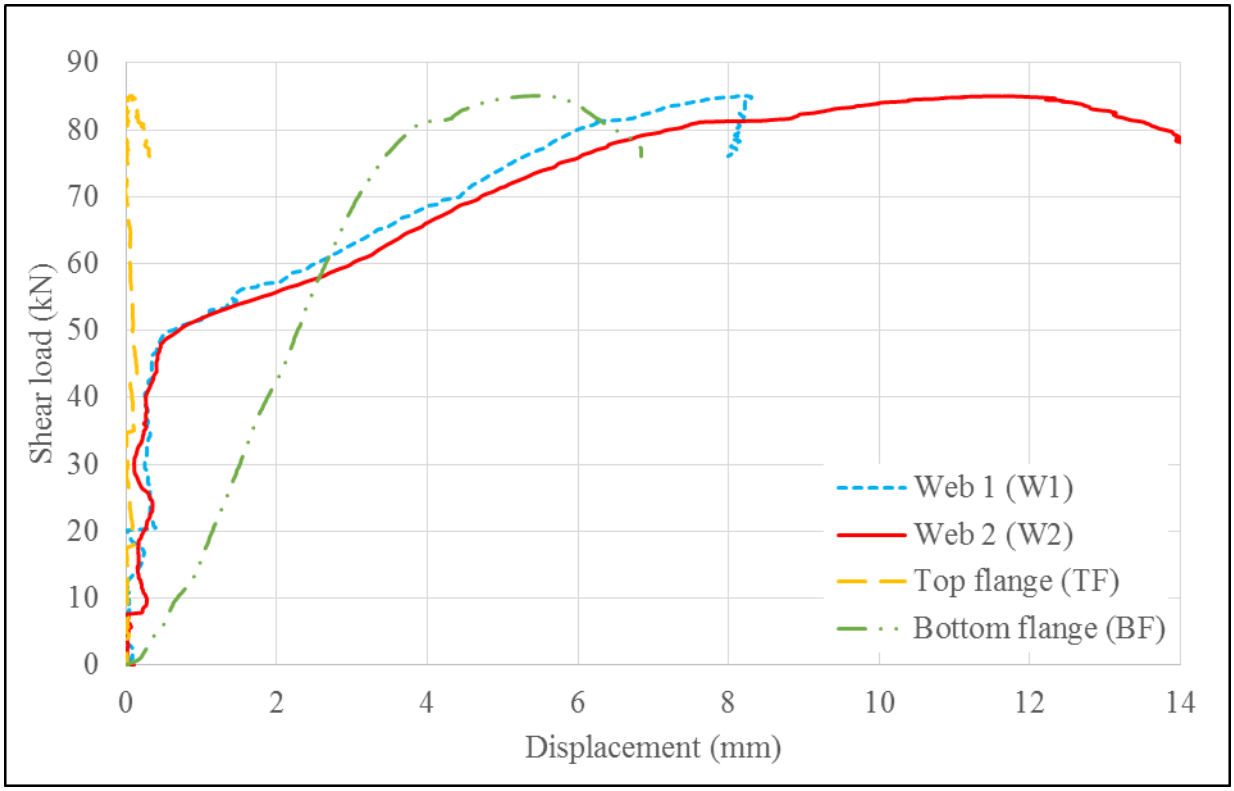

Figure 12: Load versus displacement curves of specimen 35030-2WSP-8AS-2VRB.

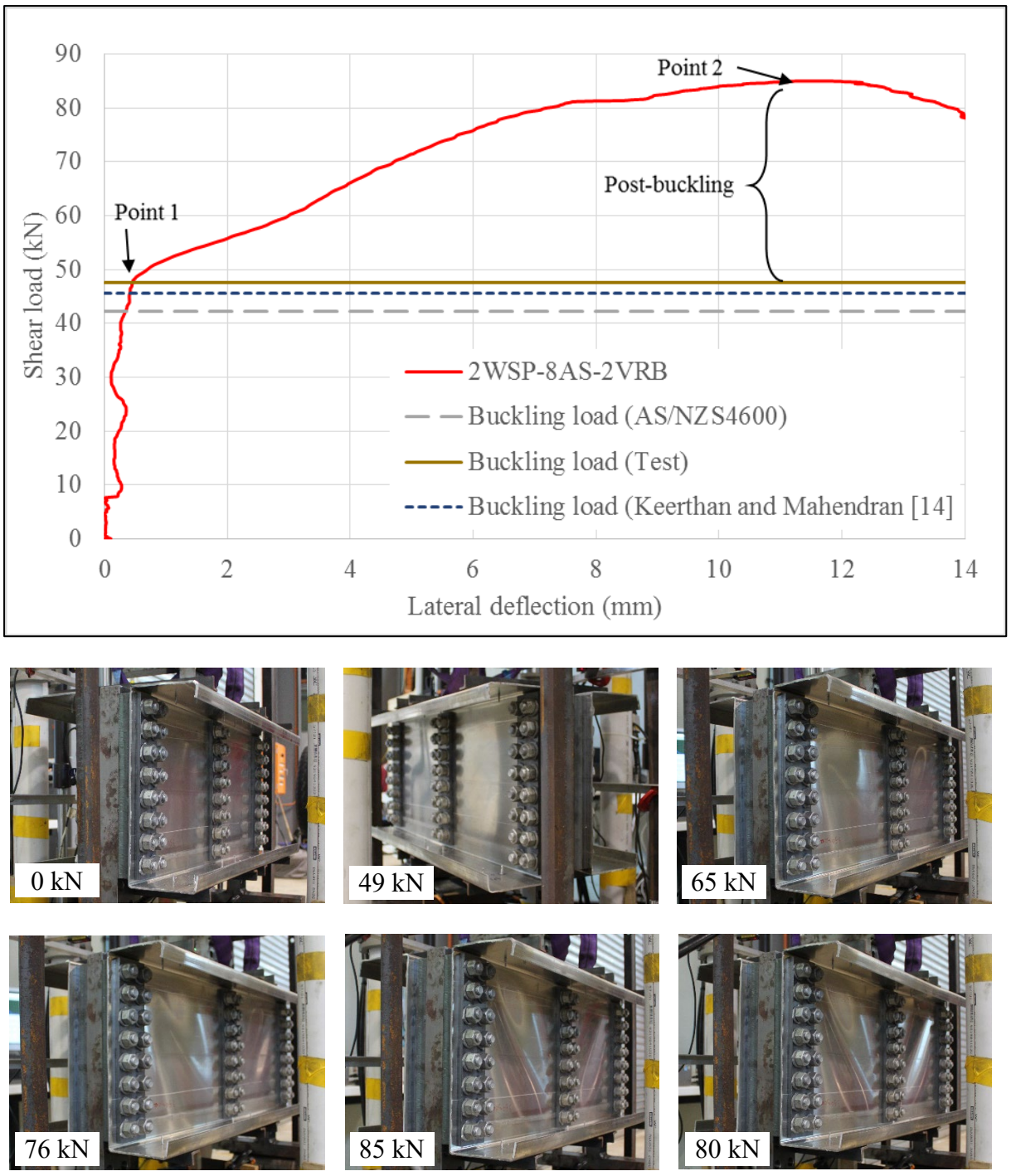

Figure 13: Post buckling strength of Section 35030.

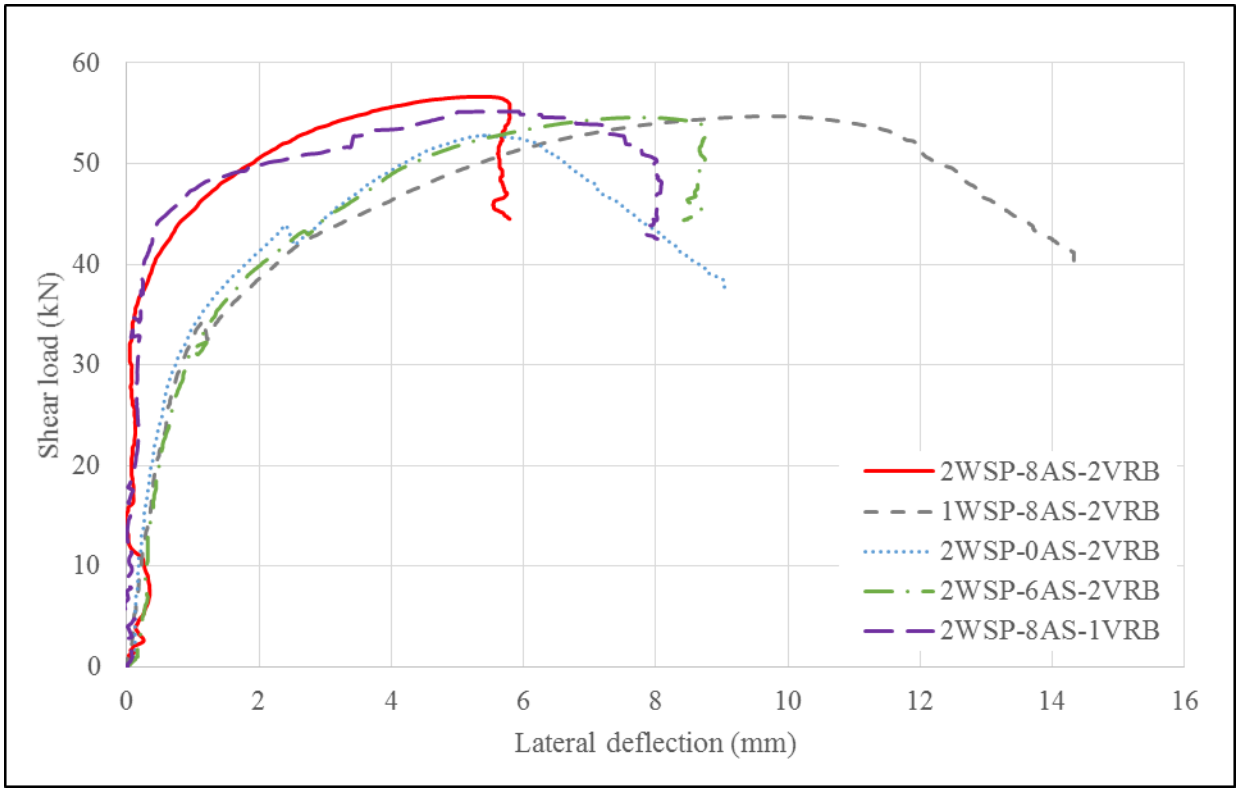

Figure 14: Load versus lateral deflection of Section 25025 for different boundary conditions.

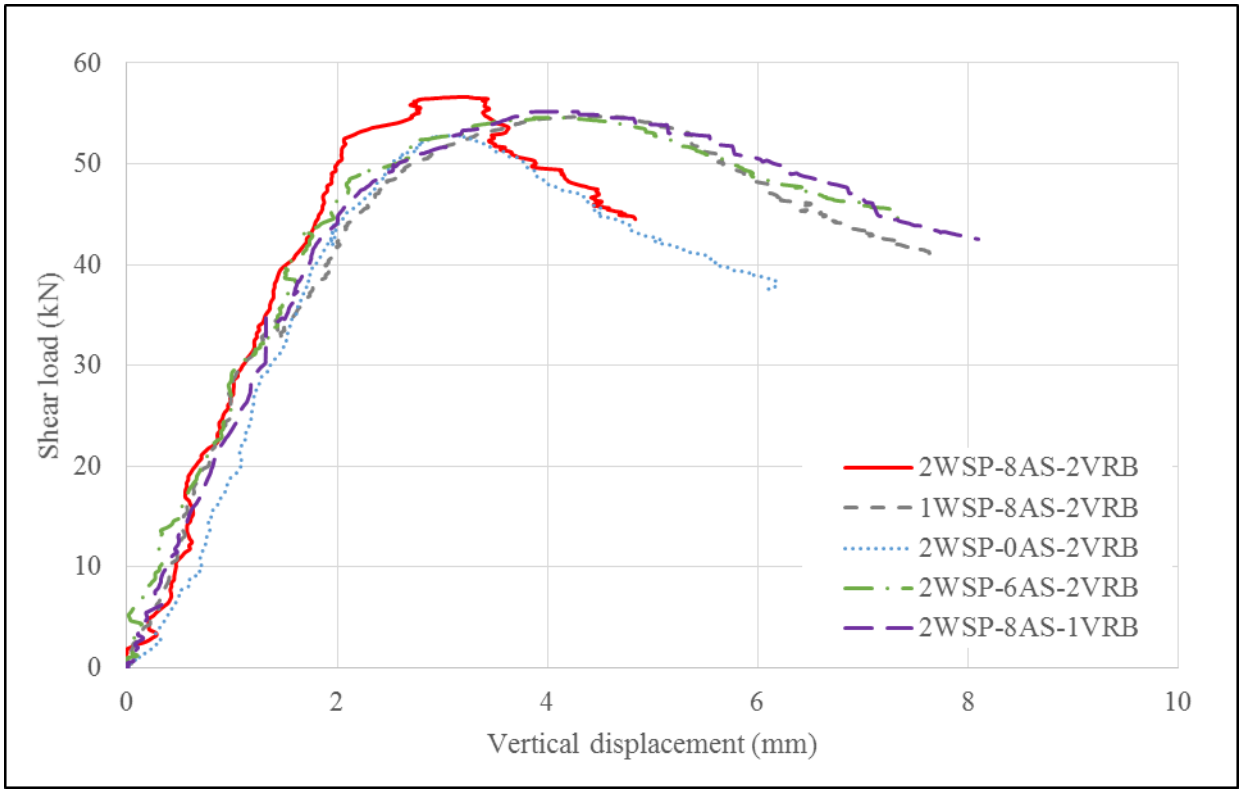

Figure 15: Load versus vertical displacement of Section 25025 for different boundary conditions.

(a) 2WSP-8AS-2VRB

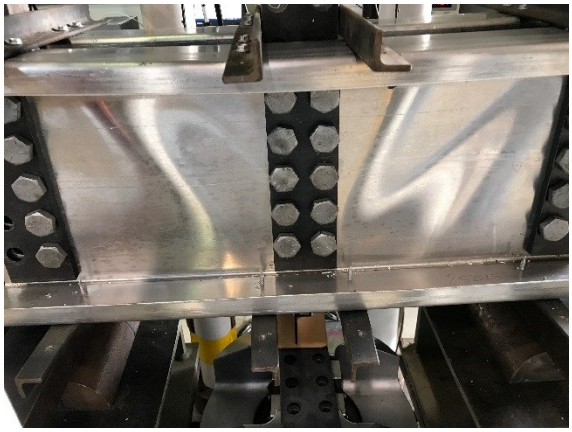

(b) 2WSP-8AS-**1VRB**

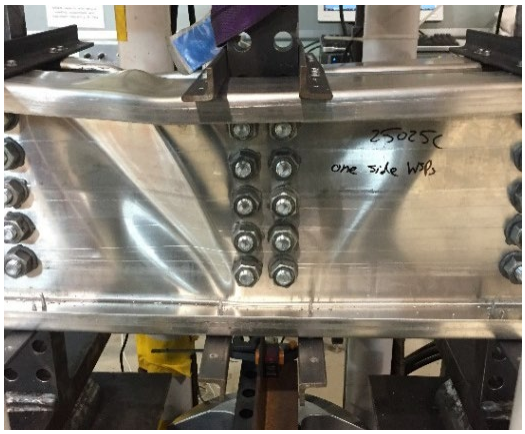

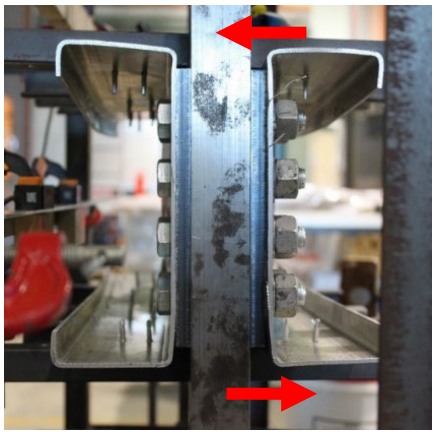

(c) **1WSP**-8AS-2VRB

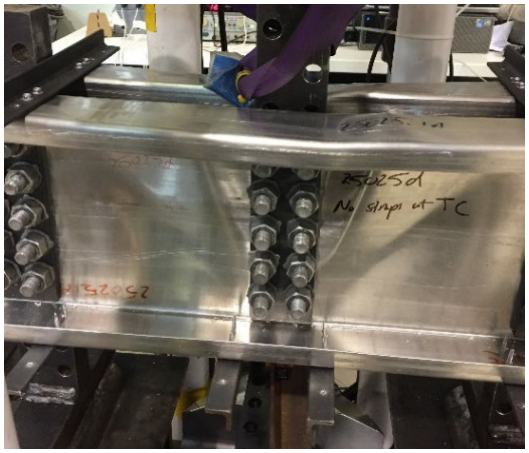

(d) 2WSP-**0AS**-2VRB

(e) 2WSP-**6AS**-2VRB

Figure 16: Shear failure modes of Section 25025 in five different test set-ups.

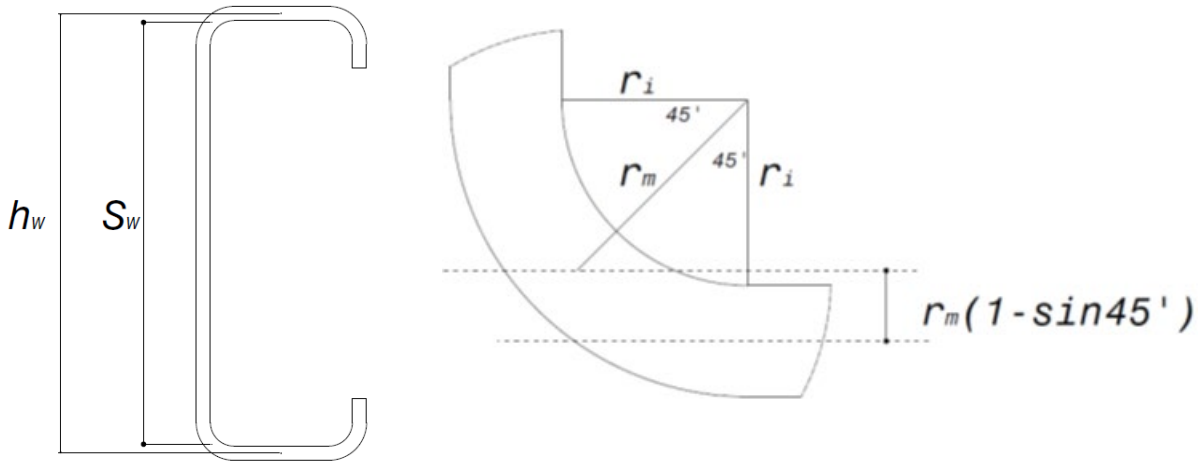

Figure 17: Dimensions for Eurocode 9 [24].

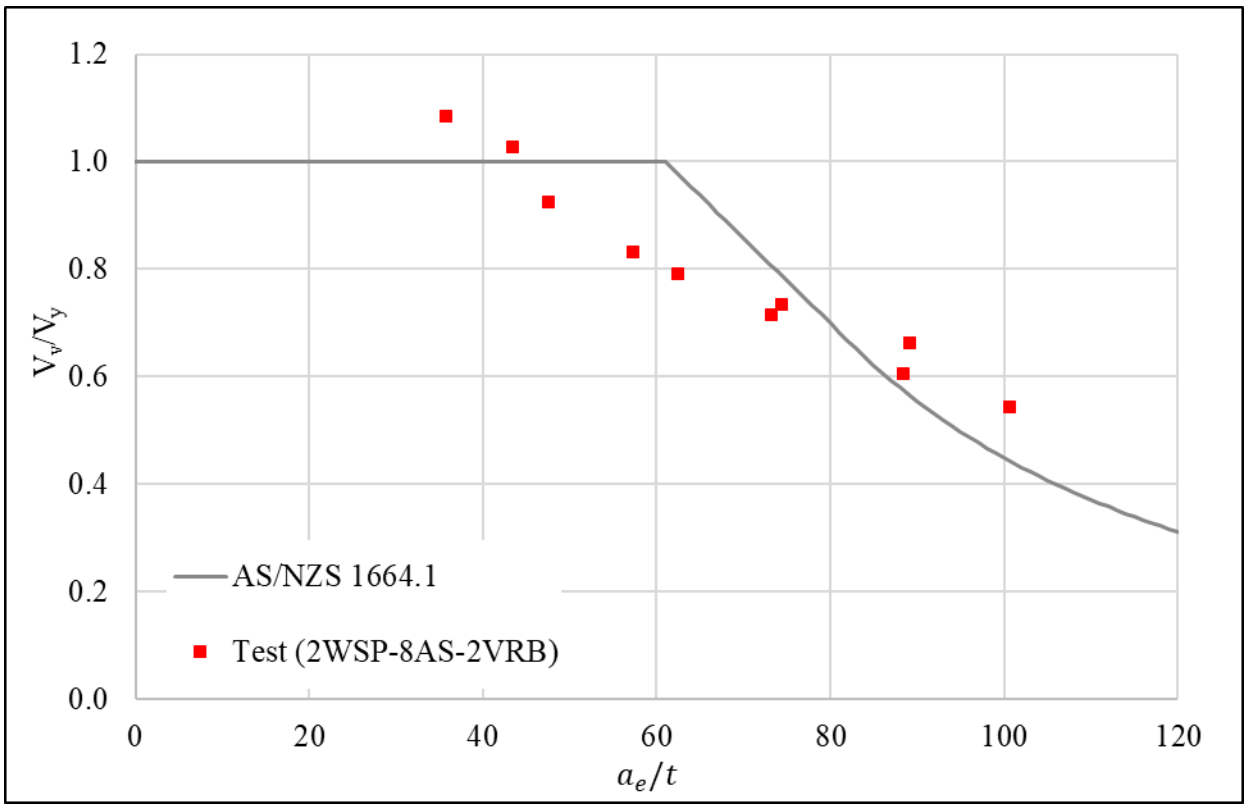

Figure 18: Comparison of test results with current AS/NZS 1664.1 [23] shear design rules.

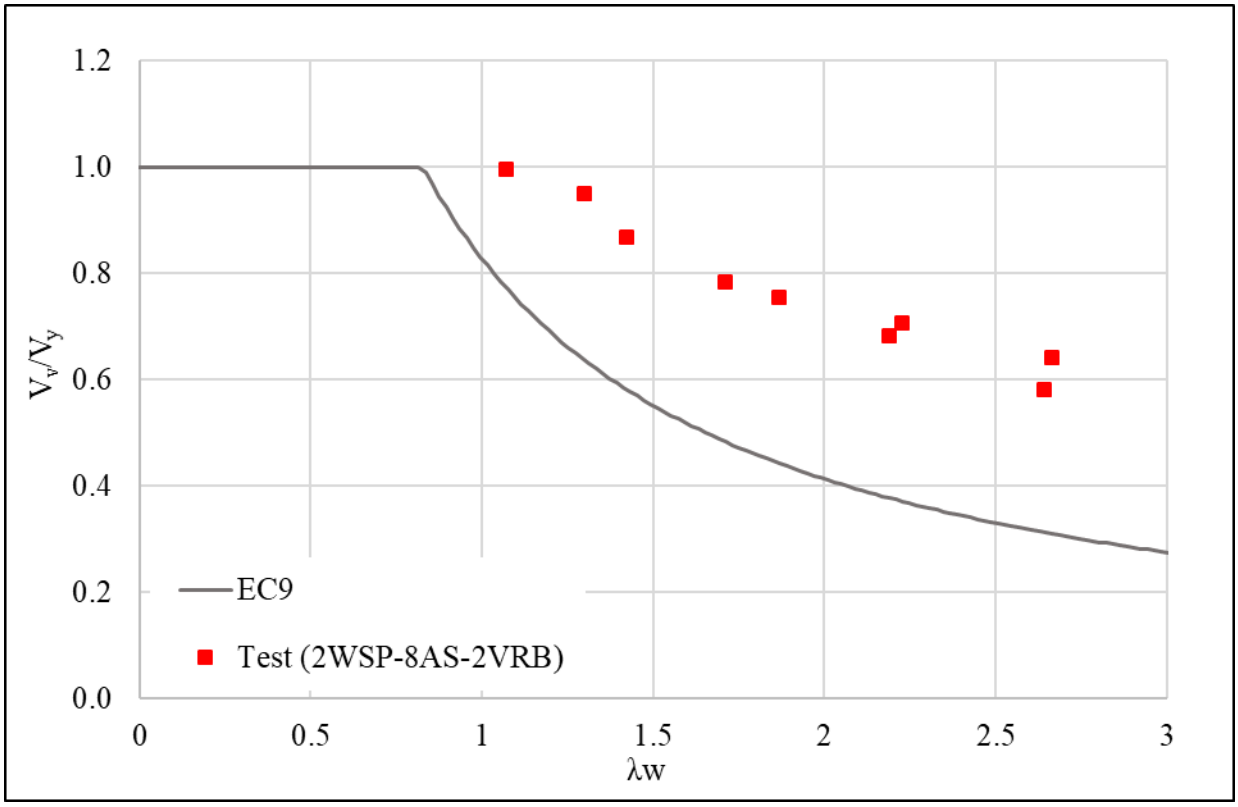

Figure 19: Comparison of test results with current Eurocode 9 [24] shear design rules.

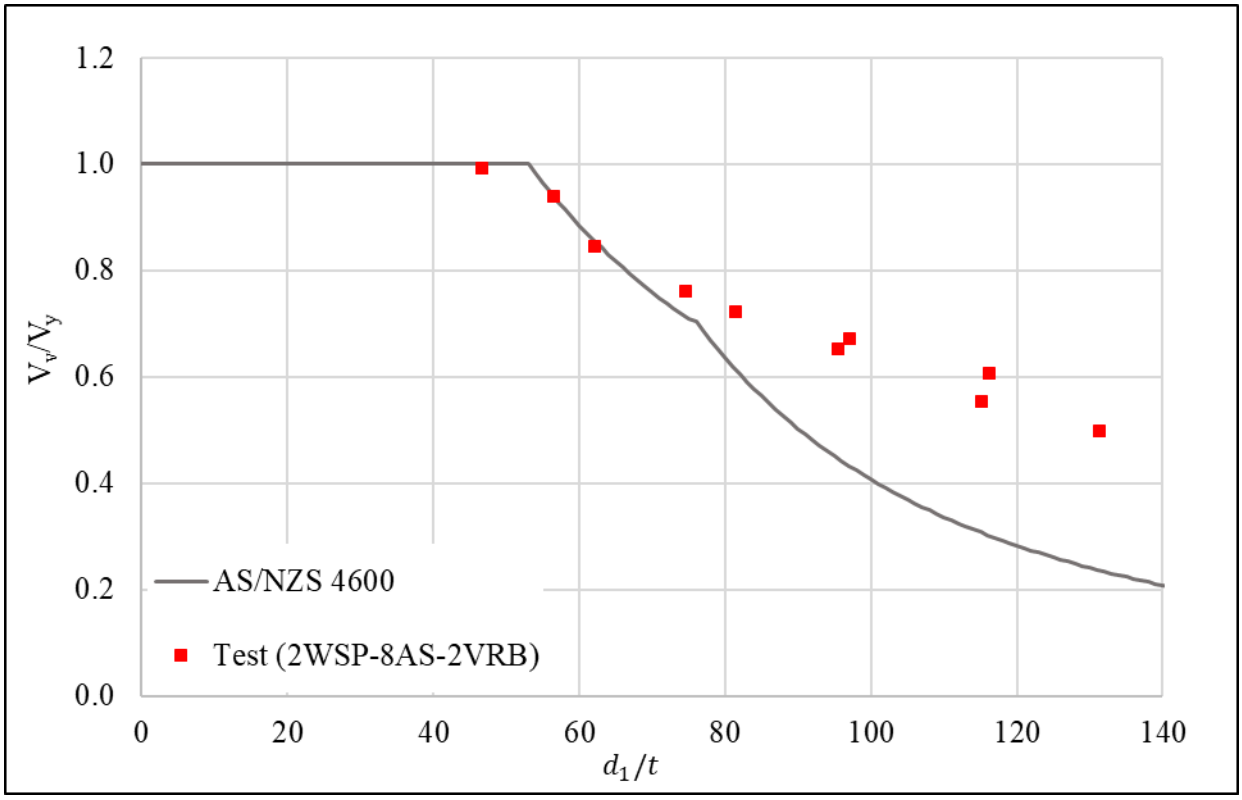

Figure 20: Comparison of test results with current AS/NZS 4600 [21] shear design rules.

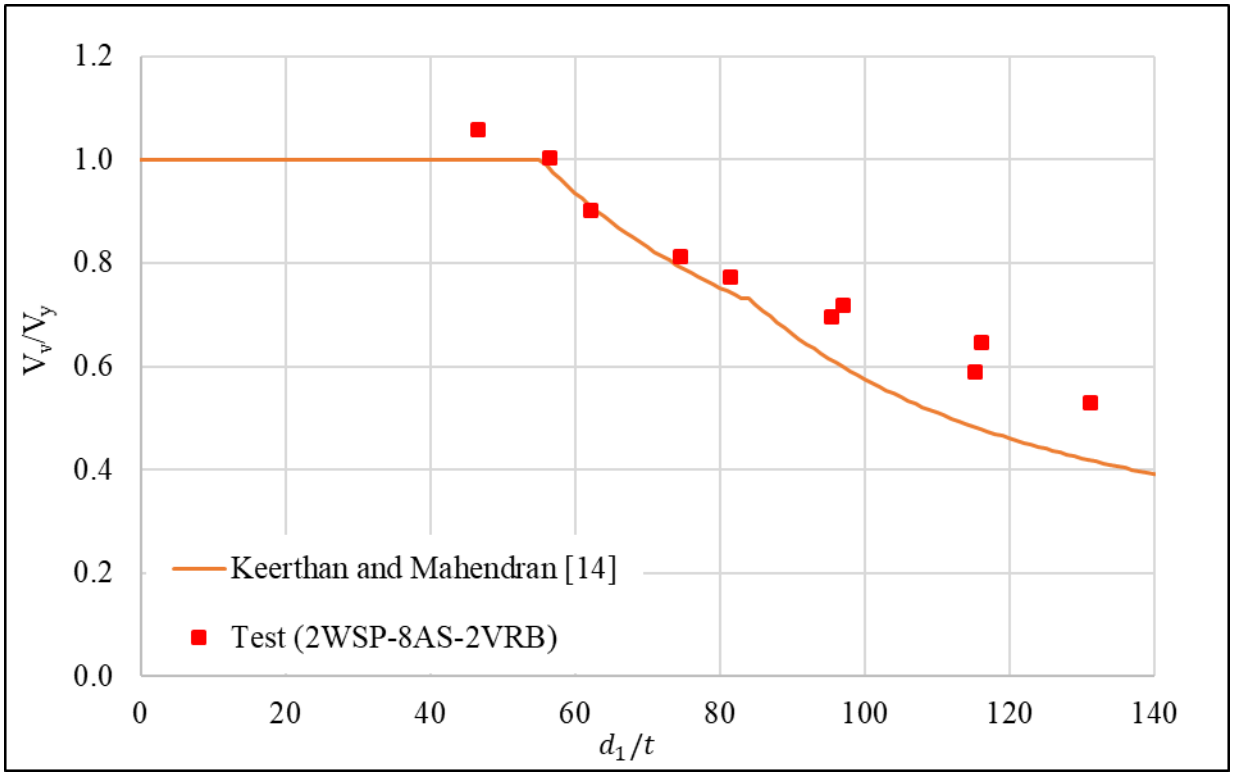

Figure 21: Comparison of test results with modified AS/NZS 4600 [14] shear design rules.

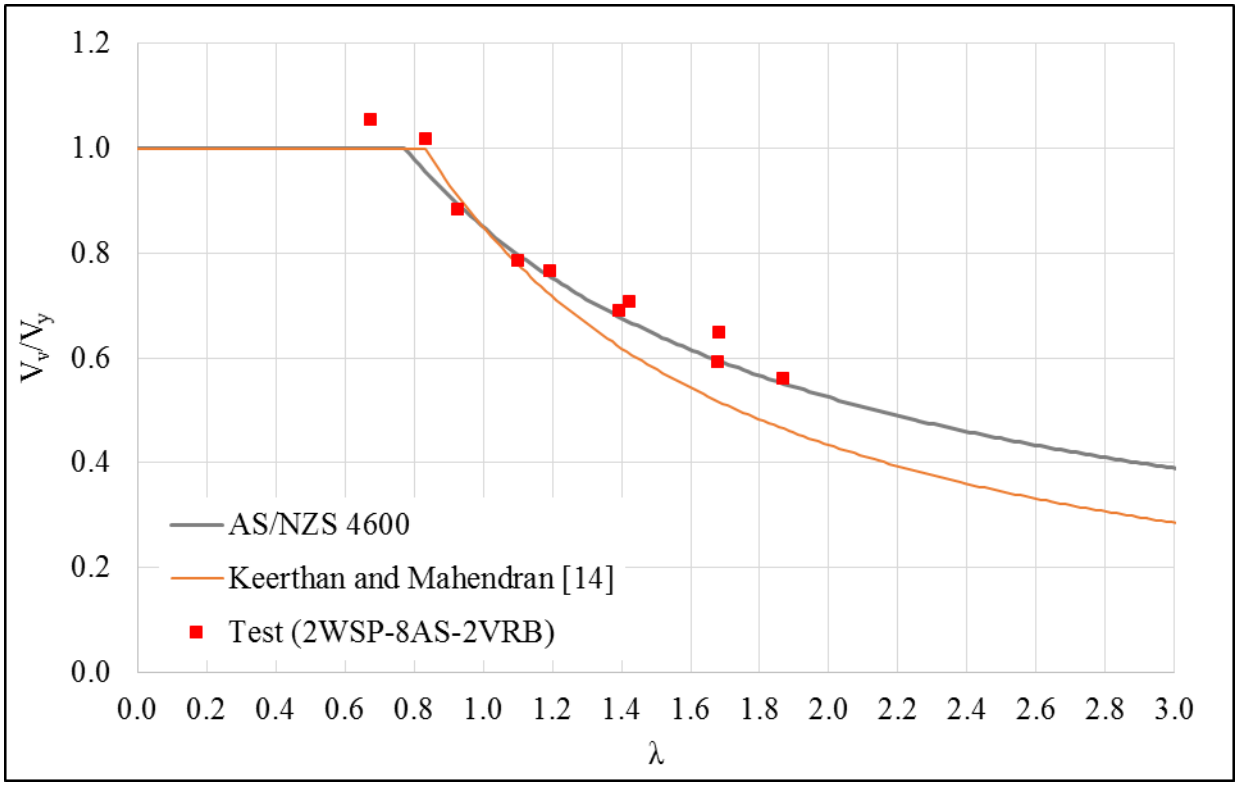

Figure 22: Comparison of test results with current DSM design rules.

Table 1: Shear test parameters.

Parameters	Number of sections tested
2WSP-8AS-2VRB	10 + 3 Repeated tests
1WSP-8AS-2VRB	6
2WSP-**0AS**-2VRB	6
2WSP-**6AS**-2VRB	2
2WSP-8AS-**1VRB**	1
Total number of tests	28

Table 2: Geometric properties of aluminium LCB specimens.

Section	Parameters	Web height D (mm)	Flange width B (mm)	Lip depth L (mm)	Web thickness t (mm)	Internal radius r_i (mm)
15025	2WSP-8AS-2VRB	155.1	61.9	22.8	2.47	5.1
15025^{R}		155.1	61.9	22.8	2.47	5.1
15030		155.2	63.1	23.4	2.97	5.3
15030^{R}		155.2	63.1	23.4	2.97	5.3
20025		204.5	75.1	23.1	2.53	5.2
20030		205.3	75.2	23.8	3.03	5.4
25025		255.4	76.1	25.4	2.51	5.2
25030		255.9	77.1	26.1	2.94	5.1
30025		302.5	110.9	29.5	2.49	5.2
30030		303.4	111.2	30.02	2.95	5.4
35030		352.1	126.5	28.2	2.89	5.1
35030^{R}		352.1	126.5	28.2	2.89	5.1
40030		405.2	125.2	29.9	2.95	5.9
15030	1WSP-8AS-2VRB	155.1	62.9	23.6	2.99	5.1
20025		205.9	75.8	25.1	2.48	5.2
20030		205.9	77.9	25.8	3.02	5.2
25025		255.5	76.2	25.6	2.53	5.5
35030		352.1	126.4	29.1	2.98	5.1
40030		404.3	127.2	30.2	3.02	5.4
15030	2WSP-0AS-2VRB	154.9	63.2	23.3	3.01	5.4
20025		205.3	75.8	24.3	2.51	5.3
20030		205.8	77.7	25.2	3.01	5.1
25025		255.4	76.1	25.52	2.49	5.2
35030		353.2	125.9	30.3	3.02	5.4
40030		403.6	126.8	29.5	2.93	5.3
20030	2WSP-6AS-2VRB	205.7	77.4	25.2	2.98	5.3
25025		255.2	75.8	25.4	2.47	5.2
25025	2WSP-8AS-1VRB	255.1	75.6	25.3	2.49	5.1

R: Repeated test

Table 3: Material properties of aluminium LCBs.

Sections	15025	15030	20025	20030	25025	25030	30025	30030	35030	40030
E (MPa)	67282	69566	68885	65689	66170	68488	67468	68301	68776	67862
f_y (MPa)	220	225	234	228	228	224	220	226	224	213
f_u (MPa)	270	272	279	271	275	275	274	277	274	266

Table 4: Ultimate loads of aluminium LCBs for 2WSP-8AS-2VRB boundary condition.

Section	V_{ult} (kN)
15025	47.80
15025^{R}	45.79
15030	58.65
15030^{R}	59.04
20025	52.44
20030	69.53
25025	56.65
25030	73.47
30025	56.91
30030	81.86
35030	85.01
35030^{R}	84.37
40030	81.76

R: Repeated test

Table 5: Ultimate loads of aluminium LCBs and the effect of boundary conditions.

Section	1WSP-8AS-2VRB		2WSP-0AS-2VRB		2WSP-6AS-2VRB		2WSP-8AS-1VRB	
	V_{ult} (kN)	Ratio$^{\#}$	V_{ult} (kN)	Ratio$^{\#}$	V_{ult} (kN)	Ratio$^{\#}$	V_{ult} (kN)	Ratio$^{\#}$
15030	53.64	0.91	49.66	0.84	-	-	-	-
20025	50.50	0.96	48.13	0.92	-	-	-	-
20030	66.68	0.96	64.50	0.93	67.58	0.97	-	-
25025	54.64	0.96	52.81	0.93	54.54	0.96	55.20	0.97
35030	80.45	0.95	77.57	0.92	-	-	-	-
40030	78.12	0.96	71.05	0.87	-	-	-	-

#: Ratio of ultimate loads compared to 2WSP-8AS-2VRB

Table 6: Comparison of test results with current design rules for 2WSP-8AS-2VRB.

Section	V_{ult} (kN)							V_{ult} (Test) / V_{ult} (Predicted)					
	Test	[23]	[24]	[21]	[14]	[21, 26]*	[14]*	[23]	[24]	[21]	[14]	[21, 26]*	[14]*
15025	46.80	45.58	33.99	46.76	45.80	42.96	46.05	1.03	1.38	1.00	1.02	1.09	1.02
15030	58.85	54.30	49.24	59.41	55.69	55.80	55.84	1.08	1.20	0.99	1.06	1.05	1.05
20025	52.44	63.06	35.46	49.06	51.18	51.89	51.95	0.83	1.48	1.07	1.02	1.01	1.01
20030	69.53	75.29	50.93	70.37	70.30	68.66	71.72	0.92	1.37	0.99	0.99	1.01	0.97
25025	56.65	63.95	34.77	38.70	49.74	54.17	50.99	0.89	1.63	1.46	1.14	1.05	1.11
25030	73.47	90.73	47.72	62.23	70.71	70.57	69.23	0.81	1.54	1.18	1.04	1.04	1.06
30025	56.91	54.09	34.14	31.58	46.63	55.65	49.75	1.05	1.67	1.80	1.22	1.02	1.14
30030	81.86	87.66	47.95	52.59	68.33	75.32	70.51	0.93	1.71	1.56	1.20	1.09	1.16
35030	84.69	72.24	45.91	42.18	62.72	75.41	67.34	1.17	1.84	2.01	1.35	1.12	1.26
40030	81.76	66.64	47.82	38.91	64.55	78.34	67.93	1.23	1.71	2.10	1.27	1.04	1.20
Mean value								0.99	1.55	1.42	1.13	1.05	1.10
COV								0.142	0.128	0.307	0.109	0.035	0.084

*Note: Direct Strength Method

Table 7: Comparison of test results with modified design rules for 1WSP-8AS-2VRB and 2WSP-0AS-2VRB.

Section	1WSP-8AS-2VRB			2WSP-0AS-2VRB		
	V_{ult} (Test) (kN)	0.95 x V_{ult} (kN) DSM [21, 26]	V_{ult} (Test) / V_{ult} (Predicted)	V_{ult} (Test) (kN)	0.90 x V_{ult} (kN) DSM [21, 26]	V_{ult} (Test) / V_{ult} (Predicted)
15030	53.64	53.04	1.01	49.66	50.28	0.99
20025	50.5	49.32	1.02	48.13	46.75	1.03
20030	66.68	65.26	1.02	64.50	61.87	1.04
25025	54.64	51.49	1.06	52.81	48.81	1.08
35030	80.45	71.68	1.12	77.57	67.95	1.14
40030	78.12	74.47	1.05	71.05	70.59	1.01
Mean value			1.05			1.05
COV			0.039			0.053